International Journal of Heat and Mass Transfer 249 (2025) 127198

Contents lists available at ScienceDirect

International Journal of Heat and Mass Transfer

journal homepage: www.elsevier.com/locate/hmt

Solution of the extended Graetz problem for nonuniform heat flux

Jonathan Neuhauser *, Jan-Henrik Metsch, Davide Gatti, Bettina Frohnapfel

Institute of Fluid Mechanics, Karlsruhe Institute of Technology, Kaiserstr. 10, Karlsruhe, Germany

ARTICLE INFO

Dataset link: https://github.com/joneuhauser/graetz/

Keywords:
Heat transfer
Analytical solution
Graetz problem
Laminar flow

ABSTRACT

Pipe flows subject to azimuthally non-uniform heat flux are present in e.g. concentrated solar power plants. In this paper, we present novel analytical solutions for this configuration under laminar flow conditions, namely the fully developed solution (including conjugate heat transfer) as well as the thermal entrance behavior, both with and without the effect of axial conduction. The solution is obtained by additively decomposing the temperature field into Fourier modes, owning to the linearity of the conservation equation of temperature. The solution for each wavenumber is then expanded in terms of eigenfunctions of a linear self-adjoint operator. The eigenfunctions of said operator can be stated explicitly for a laminar velocity profile. For negligible axial conduction (large values of the Péclét number Pe), the coefficients of the eigenfunction expansion are determined analytically from the eigenvalues. For finite values of Pe, the coefficients are obtained as solutions of a quadratic matrix equation, which are constructed explicitly and show to be well-behaved. We show that global quantities like the mean Nusselt number are independent of the heat flux distribution. However, the pointwise temperature is significantly changed; especially for variations with a wavelength of 2π (the thermal entrance length of the $k = 1$ mode is between 2.2 and 2.7 times longer than for the homogeneous case, depending on Pe). The presented analytical solutions are verified against numerical data.

1. Introduction

The balance of convection and diffusion governs the analysis of any transfer problem of heat or mass, and it is typically formulated as a boundary value problem. An important class of solutions considers the steady state, and one relevant example is the so-called *Graetz problem*, which is the analysis of the thermal entrance region for heat transfer in a laminar flow through a given geometry, either subject to uniform wall heat flux or uniform temperature. Following the fundamental paper by Graetz [1], who solved the heat transfer problem in the thermal entrance region for the case of pipe flow with prescribed wall temperature and negligible axial conduction,[1] a wealth of literature has since been produced to extend these results to more complex cases.

For liquid metal flows (low values of Pr) or flows of small physical lengthscales, the relative importance of axial conduction is raised with respect to the effect of axial convection, and hence Graetz' original solution is not valid anymore. The relationship between those two quantities is expressed in the non-dimensional Péclét number Pe. For relatively low values of Pe, say Pe $<$ 70 [2], axial conduction must be considered in the formulation, which is then termed the *extended* Graetz problem. In a series of articles, Papoutsakis et al. [2,3] presented the first fully analytical solution to the extended Graetz problem, based on introducing a secondary variable and then reformulating the problem using a self-adjoint operator. It should be noted that Graetz's solution (and derived ones, such as [3]) in terms of an orthogonal series expansion usually converges very quickly except in close proximity to the inlet. There a large number of eigenfunctions are required for sufficient accuracy, and hence, Lévêque's solution is a more suitable approximation [4].

Analytical solutions of heat transfer in pipe flows typically consider uniform heat flux, i.e. the problem becomes independent of the azimuthal coordinate. However, azimuthally inhomogeneous heat flux, also termed nonuniform heat flux, is present in relevant technical applications, such as heat exchangers or concentrated solar power plants. A simpler subproblem considers the thermally fully developed solution, i.e. where the temperature is considered invariant of the streamwise direction after suitable non-dimensionalization. This state is (approximately) reached sufficiently far away from the start of the heated section. The fully-developed solution for nonuniform heating is given by W. Reynolds [5], and Gatewood [6, equation 6.3] gives the basic form of the fully developed solution for the conjugated problem. To the authors' knowledge, a solution for the thermal entrance region subject to azimuthally inhomogeneous heating has not yet been reported. This gap in the existing literature is adressed in the present article.

* Corresponding author.
E-mail address: jonathan.neuhauser@kit.edu (J. Neuhauser).

[1] Graetz already included the heat conduction inside a solid (conjugated problem).

https://doi.org/10.1016/j.ijheatmasstransfer.2025.127198
Received 17 February 2025; Received in revised form 19 April 2025; Accepted 29 April 2025
Available online 22 May 2025

Nomenclature

The nomenclature only includes symbols required for the main text and does not include those exlusively used in Appendix B.

Latin symbols

A_k	Matrix-valued coefficient of the exponential function for the finite Pe solution (Eq. (47))
A_k^+, A_k^-	Solutions A_k identified with $z < 0$ and $z < 0$, respectively (Eq. (50))
a_{kj}, b_k	Parameters of the Eigenfunction (Eq. (39)
$C_i, A_{k,p}, B_{k,p}$	Integration constants
C_k	Diagnostic quantity for the thermal entrance length (Eq. (43))
c_k	Vector of expansion coefficients (Eq. (46))
c_{kj}	Coefficients of the eigenfunction expansion (Eq. (32))
c_p	Specific heat capacity at constant pressure
d	Jump condition for the derivative of the expansion coefficient (Appendix C)
D	Space of the linear operator $\mathcal{L}_k$ (Eq. (26))
$D_{\lvert k\rvert}$	Fully developed solution for wavenumber k (Eq. (20))
$f(\varphi)$	Azimuthal heat flux after removal of the mean q_w (Eq. (2c))
f_k	kth complex Fourier coefficient of $f(\varphi)$
H^2	Sobolev space of square-integrable functions with square-integrable first and second derivatives
j	Imaginary unit
k	Wavenumber
$\mathcal{L}$	Self-adjoint linear operator (Eq. (25))
M	Confluent Hypergeometric Function ${}_1F_1$
p_k	Function to transform the wavenumber solution into D (Eq. (28))
$\overline{p}_k$	The image of p_k under the operator $\mathcal{L}_k$ (Eq. (28))
q_w	Azimuthal mean of the heat flux (Eq. (2c))
q_k	Jump condition for the expansion coefficient; right hand side of Eq. (*35)
r	Radial coordinate
$\mathbb{R}$	Set of real numbers
R_i	Radius of the pipe's inner wall
R_o	Radius of the pipe's outer wall
T	Temperature
T_0	Inlet temperature (Eq. (2b))
u, v	Example functions (Eq. (27))
U_{ref}	Reference velocity for non-dimensionalization (Eq. (4))
u_z	Streamwise velocity
z	Streamwise coordinate

Greek symbols

Γ	Ratio of radii, $\Gamma = R_o/R_i$
K_k	Matrix representation of the extra term in the coefficient ODE for finite Pe (Eq. (46))
λ	Thermal conductivity
λ_{sf}	Solid/Fluid ratio of conductivities
λ_{kj}	Eigenvalue corresponding to the jth eigenfunction of $\mathcal{L}_k$
Λ_k	Diagonal matrix of eigenvalues (Eq. (46))
μ_{kj}	Square root of the negated value of λ_{kj}
ϕ_{kj}	jth normalized eigenfunction of $\mathcal{L}_k$
φ	Azimuthal coordinate
$\Pi_{\lvert k\rvert}$	Auxiliary quantity, see Eq. (20)
ρ	Density
$\overline{\theta}$	Dimensionless temperature after subtraction of the linear increase in z (fully developed solution, see Eq. (8))
$\tilde{\theta}_k$	Fourier mode of dimensionless temperature (Eq. (12))
$\hat{\theta}_k$	Transformed Fourier mode of dimensionless temperature, i.e. $\hat{\theta}_k \in D_k$ (Eq. (28))
θ	Dimensionless temperature (Eq. (4))

Subscripts

$\square_f$	Fluid
$\square_k$	Quantity associated with wavenumber k
$\square_p$	Phase (p being fluid f or solid s)
$\square_s$	Solid

Superscripts

$\square^*$	Complex conjugate (from Section 2.2 on)
$\square^*$	Non-dimensionalized quantity (only in Section 2.1). The superscript is omitted starting with Section 2.2.

Abbreviations

Im	Imaginary part of complex number
Pe	Péclét number (Eq. (4))
Pr	Prandtl number, $\text{Pr} = \mu_f/(c_{p,f}\lambda_f)$
Re	Real part of complex number

This paper treats heat transfer in laminar pipe flows. In other geometries, asymmetric heating of a plane channel has been considered [7,8], and experimental results for asymmetric heating of a square duct have been reported [9]. Related to the latter case, Barrera et al. [10] solved the (regular) Graetz problem for homogeneous heating condition on non-circular cross section. Some interesting mathematical similarities between Barrera et al. [10] and the present formulation arise and will be discussed in Section 2.3.

In this paper, we present the solution for the nondimensional temperature in a non-uniformly heated pipe under standard laminar flow conditions. The paper is structured as follows: after introducing the governing equations in Section 2.1, we summarize the fully developed solution for nonuniform heating in Section 2.2, including conjugate heat transfer. We then turn our attention to the thermal development region and present the solution to the Graetz problem (negligible axial conduction) in Section 2.3. The solution is modified to accommodate finite Pe numbers in Section 2.4.

2. Analysis

2.1. Governing equations

We consider an incompressible Newtonian fluid with constant material properties in a thick-walled pipe under laminar flow conditions. Heating through viscous dissipation, thermal expansion and radiation is neglected. We assume constant material properties for the fluid (index 'f') and solid (index 's') phases, respectively.

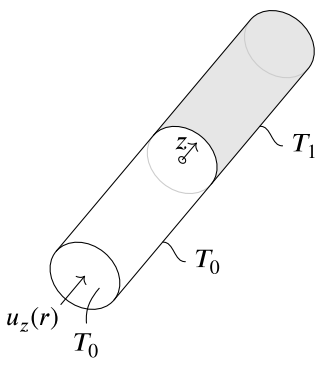

(a) Graetz problem with Dirichlet boundary conditions

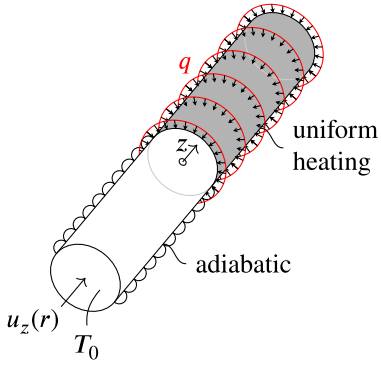

(b) Graetz problem with homogeneous Neumann boundary conditions

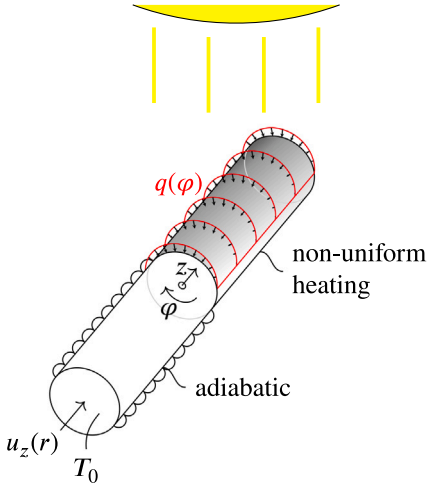

(c) Graetz problem with inhomogeneous Neumann boundary conditions

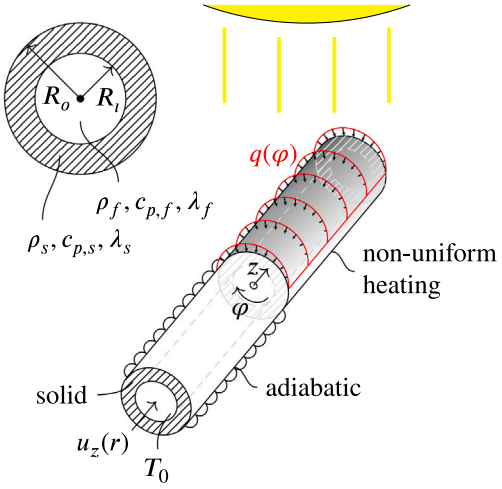

(d) Conjugated Graetz problem with inhomogeneous Neumann boundary conditions

Fig. 1. Sketch of the typical configurations of the Graetz problem (Figs. 1(a) and 1(b)), as well as the non-uniform heating case (Fig. 1(c)) and conjugated case (Fig. 1(d)) considered in this paper.

We denote the streamwise coordinate with z, the radial coordinate with r and the azimuthal coordinate with φ. The solid has an inner diameter R_i and an outer diameter R_o, see also sketch Fig. 1(d).

The steady-state balance equation of temperature T_p (p / phase being fluid or solid) is given by [11, Appendix B.9]

$$\rho_f c_{p,f} u_z(r) \frac{\partial T_f}{\partial z} = \frac{\lambda_f}{r}\frac{\partial}{\partial r}\left(r\frac{\partial T_f}{\partial r}\right) + \frac{\lambda_f}{r^2}\frac{\partial^2 T_f}{\partial \varphi^2} + \lambda_f \frac{\partial^2 T_f}{\partial z^2} \quad \text{fluid,} \tag{1a}$$

$$0 = \frac{\lambda_s}{r}\frac{\partial}{\partial r}\left(r\frac{\partial T_s}{\partial r}\right) + \frac{\lambda_s}{r^2}\frac{\partial^2 T_s}{\partial \varphi^2} + \lambda_s \frac{\partial^2 T_s}{\partial z^2} \quad \text{solid,} \tag{1b}$$

where ρ, c_p and λ denote density, specific heat capacity at constant pressure and thermal conductivity, respectively. Viscous dissipation is neglected. Note that only conduction is present in the solid, while both convection and diffusion are considered in the fluid. The boundary conditions are given by

$$\lim_{z\to-\infty} T_p(r,\varphi,z) = T_0, \quad \text{for a constant } T_0, \tag{2a}$$

$$T_f(0,\varphi,z) \text{ is regular in } z \text{ and } \varphi, \tag{2b}$$

$$\lambda_s \left.\frac{\partial T_s}{\partial r}\right|_{R_o} = \begin{cases} q_w + f(\varphi) & \text{for } \varphi \in [0,2\pi) \text{ and } z \geq 0, \\ 0 & \text{for } \varphi \in [0,2\pi) \text{ and } z < 0. \end{cases} \tag{2c}$$

These are the same boundary conditions used in [2], except with the addition of azimuthal inhomogeneity in the heat flux. Here q_w is the mean contribution of heat flux, that is, $\int_0^{2\pi} f(\varphi)\mathrm{d}\varphi = 0$. These boundary conditions correspond to a uniform inlet temperature T_0 far away from the beginning of the heated section (Eq. (2a)), and a prescribed heat flux on the outer wall of the pipe (Eq. (2c)). If the solid is omitted, this condition is specified on the inner pipe wall instead as a boundary condition for the fluid.

Furthermore, we impose interface conditions (see e.g. [12])

$$\lambda_s \left.\frac{\partial T_s}{\partial r}\right|_{R_i} = \lambda_f \left.\frac{\partial T_f}{\partial r}\right|_{R_i} \quad \text{for all } z \in \mathbb{R} \text{ and } \varphi \in [0,2\pi), \tag{3a}$$

$$T_f(R_i,\varphi,z) = T_s(R_i,\varphi,z) \quad \text{for all } z \in \mathbb{R} \text{ and } \varphi \in [0,2\pi). \tag{3b}$$

These reflect the conservation of energy on the interface and continuity of the temperature.

Conservation equations Eq. (1) and interface conditions Eq. (3) are a rather standard choice and are often used in analytical and numerical investigations of conjugate heat transfer. We note that there are scenarios in which this set of equations fail to capture the relevant physical effects. For example, viscous dissipation is typically non-negligible in microchannels; the extended Graetz problem for this case was investigated by [13], which also discussed the influence of different inlet boundary conditions other than Eq. (2b). The fluid-solid interface condition may also be altered: an imperfect interface can introduce a nonzero thermal contact resistance, or radiative effects may be relevant [14].

It is common to express equations and solution in dimensionless form as ultimately this leads to a formulation that depends on fewer free parameters. To this end, each physical variable is expressed as the

product of a dimensionless variable and a dimensional reference quantity of the same unit. Here, we denote the conductivity ratio $\lambda_{sf} = \frac{\lambda_s}{\lambda_f}$. The ratio of radii is indicated by $\Gamma = \frac{R_o}{R_i}$. The non-dimensionalization employed in the following is given by

$$\theta_p = \frac{T_p - T_0}{q_w \Gamma R_i / \lambda_f}, \qquad z = \mathrm{Pe} R_i z^*, \qquad r = R_i r^*, \tag{4a}$$

$$\mathrm{Pe} = \frac{\rho_f c_{p,f} U_{\mathrm{ref}} R_i}{\lambda_f}, \qquad u_z = U_{\mathrm{ref}} u_z^*. \tag{4b}$$

The non-dimensionalization follows [2] with the addition of conjugate heat transfer. Note that the choice of different length scales in axial and radial directions enables to characterize the relevance of axial conduction relative to axial convection, and the occurrence of Γ in the non-dimensionalization of T will later ensure that the circumferentially averaged heat flux on the fluid is 1.

Expressions Eq. (4) are then inserted into the equation (1) and boundary conditions Eqs. (2) and (3), and dimensional reference quantities combined to obtain from Eq. (1):

$$\frac{1}{r^*}\frac{\partial}{\partial r^*}\left(r^*\frac{\partial \theta_p}{\partial r^*}\right) + \frac{1}{(r^*)^2}\frac{\partial^2 \theta_p}{\partial \varphi^2} + \frac{1}{\mathrm{Pe}^2}\frac{\partial^2 \theta_p}{\partial (z^*)^2} = \begin{cases} u_z^*(r^*)\frac{\partial \theta_f}{\partial z^*} & \text{fluid,} \\ 0 & \text{solid,} \end{cases} \tag{5}$$

Using $f^*(\varphi) q_w = f(\varphi)$, the boundary conditions Eqs. (2a) and (2c) give

$$\lim_{z \to -\infty} \theta(r, \varphi, z) = 0 \qquad \text{for all } r > 0 \text{ and } \varphi \in [0, 2\pi), \tag{6a}$$

$$\left.\frac{\partial \theta_s}{\partial r^*}\right|_{r^*=\Gamma} = \frac{1}{\Gamma \lambda_{sf}} \begin{cases} 1 + f^*(\varphi) & \text{if } z \geq 0 \text{ and } \varphi \in [0, 2\pi) \\ 0 & \text{if } z < 0 \text{ and } \varphi \in [0, 2\pi), \end{cases} \tag{6b}$$

while the interface conditions Eq. (3) simply become

$$\lambda_{sf} \left.\frac{\partial \theta_s}{\partial r^*}\right|_{r^*=1} = \left.\frac{\partial \theta_f}{\partial r^*}\right|_{r^*=1} \qquad \text{for all } z \in \mathbb{R} \text{ and } \varphi \in [0, 2\pi), \tag{7a}$$

$$\theta_f(r^* = 1, \varphi, z) = \theta_s(r^* = 1, \varphi, z) \qquad \text{for all } z \in \mathbb{R} \text{ and } \varphi \in [0, 2\pi). \tag{7b}$$

For clarity of the presentation, we omit the star superscripts in the following. That is, going forward r will reference the non-dimensional radius.

2.2. Fully developed solution

The solution for the fully developed state, presented in the following, is based on [5], where the case without conjugate heat transfer is discussed.

Sufficiently far away from the start of the heated section, we expect the temperature profile to be independent of the axial position, except for a linear offset in z. This offset corresponds to the increase in bulk temperature due to the accumulated heat flux (integral energy balance). We call $\overline{\theta}_p$ the temperature profile minus the linear offset; $\overline{\theta}_p$ is then independent of z. The fully developed solution therefore takes the form

$$\theta_p = C_1 z + \overline{\theta}_p(r, \varphi) \tag{8}$$

with an integration constant C_1 (which has the same value in both subdomains). The problem at hand is given by equations Eq. (5), BCs Eqs. (2b) and (6b) and ICs Eq. (7). Boundary condition Eq. (6a) is omitted. This set of equations fully constrains the temperature profile $\overline{\theta}_p(r, \varphi)$ up to a constant offset. In order to match the behavior of the full Graetz problem (that is, including Eq. (6a)) for $z \to \infty$, we will choose it based on the integral energy balance (see [11]) between $z \to -\infty$ and z:

$$\int_0^{2\pi}\int_0^{R_o}\left(\rho c_p u_z T_p(z') - \lambda \frac{\partial T_p}{\partial z'}\right) r \mathrm{d}r\mathrm{d}\varphi \Big|_{z'=-\infty}^{z'=z} = R_o \int_0^{2\pi}\int_{-\infty}^{z} q_w \mathrm{d}z\mathrm{d}\varphi \tag{9}$$

In dimensionless form, this translates to

$$\int_0^{2\pi}\int_0^{1}\left(u_z \theta_f - \frac{1}{\mathrm{Pe}^2}\frac{\partial \theta_f}{\partial z}\right) r\mathrm{d}r\mathrm{d}\varphi - \frac{\lambda_{sf}}{\mathrm{Pe}^2}\int_0^{2\pi}\int_1^{\Gamma}\frac{\partial \theta_p}{\partial z} r\mathrm{d}r\mathrm{d}\varphi = 2\pi z. \tag{10}$$

Inserting Eq. (8) into Eq. (5) removes the axial conduction as expected:

$$\frac{1}{r}\frac{\partial}{\partial r}\left(r\frac{\partial \overline{\theta}_p}{\partial r}\right) + \frac{1}{r^2}\frac{\partial^2 \overline{\theta}_p}{\partial \varphi^2} = \begin{cases} C_1 u_z(r) & \text{fluid,} \\ 0 & \text{solid} \end{cases} \tag{11}$$

$\overline{\theta}_p$ inherits the BCs Eqs. (2b) and (6b) and ICs Eq. (7) unchanged.

As the temperature profile $\overline{\theta}_p(r, \varphi)$ must be 2π-periodic in φ, we may expand it into a Fourier series. I.e., denoting the imaginary unit by j, $\overline{\theta}_j$ can be written as a series of the form

$$\overline{\theta}_p = \sum_{k=-\infty}^{\infty} \hat{\theta}_{k,p}(r) \exp(jk\varphi). \tag{12}$$

Inserting Eq. (12) into Eq. (11) yields

$$\sum_{k=-\infty}^{\infty} \exp(jk\varphi)\left(\frac{1}{r}\frac{\mathrm{d}}{\mathrm{d}r}\left(r\frac{\mathrm{d}\hat{\theta}_{k,p}}{\mathrm{d}r}\right) - \frac{k^2}{r^2}\right) = \begin{cases} C_1 u_z(r) & \text{fluid} \\ 0 & \text{solid} \end{cases} \tag{13}$$

Both sides of Eq. (13) are Fourier series — the right hand side only contains the 0-mode. As the Fourier series is unique, we may compare coefficients and deduce

$$0 = \left(\frac{\partial^2 \hat{\theta}_{k,p}}{\partial r^2} + \frac{1}{r}\frac{\partial \hat{\theta}_{k,p}}{\partial r} - \frac{k^2}{r^2}\hat{\theta}_{k,p}\right) + \begin{cases} C_1 u_z(r) & \text{if } k = 0 \text{ and fluid,} \\ 0 & \text{otherwise} \end{cases} \tag{14}$$

It is interesting to observe that the higher modes are independent of the velocity field. The regularity constraint Eq. (2b) has two consequences:

$$\left.\frac{\partial \hat{\theta}_{0,f}}{\partial r}\right|_{r=0} = 0; \qquad \hat{\theta}_{k,f} = 0, \quad k \neq 0 \tag{15}$$

Next, let $f_k = \frac{1}{2\pi}\int_0^{2\pi} b(\varphi)\exp(-jk\varphi)\mathrm{d}\varphi$ denote the kth complex Fourier coefficient for $f(\varphi)$. As $f(\varphi)$ was chosen to have zero mean, we have $f_0 = 0$. Inserting Eq. (12) into the boundary condition Eq. (6b) and again separating modes, we find

$$\left.\frac{\partial \hat{\theta}_{k,s}(r)}{\partial r}\right|_{r=\Gamma} = \frac{1}{\Gamma \lambda_{sf}} \cdot \begin{cases} 1 & \text{if } k = 0, \\ f_k & \text{else} \end{cases} \qquad \text{for } z \in \mathbb{R} \text{ and } \varphi \in [0, 2\pi). \tag{16}$$

The ICs Eq. (7) can be treated in the same way to obtain

$$\lambda_{sf} \left.\frac{\partial \hat{\theta}_{k,s}}{\partial r}\right|_{r=1} = \left.\frac{\partial \hat{\theta}_{k,f}}{\partial r}\right|_{r=1} \qquad \text{for } z \in \mathbb{R} \text{ and } \varphi \in [0, 2\pi), \tag{17a}$$

$$\hat{\theta}_{k,f}(r = 1, \varphi, z) = \hat{\theta}_{k,s}(r = 1, \varphi, z) \qquad \text{for } z \in \mathbb{R} \text{ and } \varphi \in [0, 2\pi). \tag{17b}$$

Finally, Eq. (10) prescribes

$$\int_0^1 \left(u_z \hat{\theta}_{0,f} - \frac{1}{\mathrm{Pe}^2}\frac{\partial \hat{\theta}_{0,f}}{\partial z}\right) r\mathrm{d}r - \frac{\lambda_{sf}}{\mathrm{Pe}^2}\int_1^{\Gamma}\frac{\partial \hat{\theta}_{0,s}}{\partial z} r\mathrm{d}r = z. \tag{18}$$

For $k = 0$, the solution to the system described by Eq. (14) and BCs/ICs Eqs. (15), (16), (18), (17a) and (17b) can be computed for any concrete velocity profile $u_z(r)$. Moreover, the 5 boundary conditions also determine the constant C_1. For the laminar profile $u_z(r) = 1 - r^2$, we find $C_1 = 4$ and

$$\hat{\theta}_0 = \frac{8}{\mathrm{Pe}^2} + \frac{8\lambda_{sf}(\Gamma^2 - 1)}{\mathrm{Pe}^2} + \begin{cases} -\frac{1}{4}r^4 + r^2 - \frac{7}{24} & \text{fluid,} \\ \frac{1}{\lambda_{sf}}\ln(r) + \frac{11}{24} & \text{solid.} \end{cases} \tag{19}$$

For $k \neq 0$, the ODEs for fluid and solid modes are identical. Eq. (14)'s solutions are $\hat{\theta}_{k,p} = A_{k,p} r^{|k|} + B_{k,p} r^{-|k|}$ with suitable integration constants $A_{k,p}$ and $B_{k,p}$. These are determined from BCs/ICs Eqs. (15), (16), (17a) and (17b):

$$\hat{\theta}_{k,p} = f_k D_{|k|,p} \tag{20a}$$

$$\text{with } D_{|k|,p} = \frac{1}{\Pi_{|k|}|k|} \cdot \begin{cases} 2r^{|k|} & \text{fluid,} \\ \frac{\lambda_{sf}+1}{\lambda_{sf}} r^{|k|} + \frac{\lambda_{sf}-1}{\lambda_{sf}} r^{-|k|} & \text{solid,} \end{cases} \tag{20b}$$

$$\text{where } \Pi_{|k|} = (\lambda_{sf} + 1)\Gamma^{|k|} - (\lambda_{sf} - 1)\Gamma^{-|k|}. \tag{20c}$$

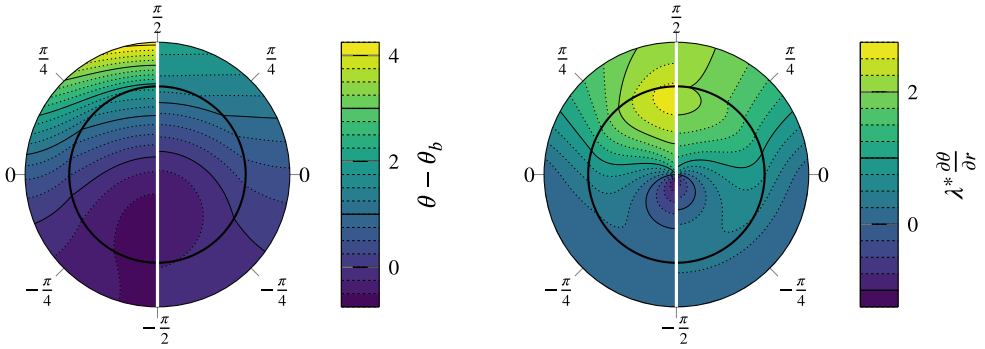

(a) Dimensionless temperature profile $\theta - \theta_b$ (b) Dimensionless radial heat flux $\lambda^* \frac{\partial \theta}{\partial r}$

Fig. 2. Fully developed solution according to Eq. (21) for half-sinusoidal heating, radii ratio $\Gamma = 1.5$ and $G_2 = 1/2$ (left semicircle) vs. $G_2 = 2$ (right semicircle). The interface between fluid and solid is indicated.

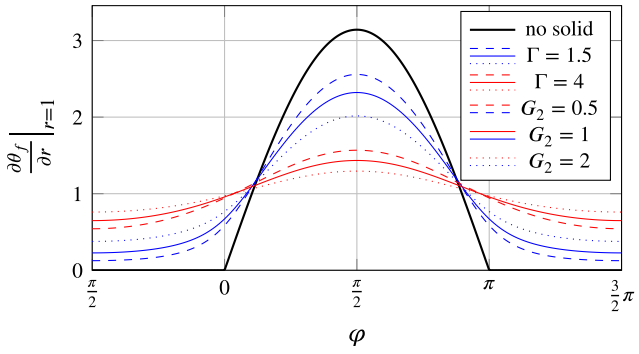

Fig. 3. Dimensionless heat flux at the interface for various values of λ_{sf} and Γ, assuming half-sinusoidal heat flux. The blue lines ($\Gamma = 1.5$) correspond to the cases displayed in Fig. 2(b). (For interpretation of the references to color in this figure legend, the reader is referred to the web version of this article.)

Note that $f_{-k} = f_k^*$ since f is real-valued. Exploiting this identity upon inserting Eqs. (19) and (20) into Eq. (12), we find

$$\theta_p = 4z + \hat{\theta}_{0,p}(r) + \sum_{k=-\infty}^{-1} \hat{\theta}_{k,p}(r)\exp(jk\varphi) + \sum_{k=1}^{\infty} \hat{\theta}_{k,p}(r)\exp(jk\varphi) \tag{21a}$$

$$= 4z + \hat{\theta}_{0,p}(r) + \sum_{k=1}^{\infty} 2D_{k,p}(\mathrm{Re}(f_k)\cos(k\varphi) - \mathrm{Im}(f_k)\sin(k\varphi)). \tag{21b}$$

In particular, the heat flux at the interface is given by

$$\left.\frac{\partial \theta}{\partial r}\right|_{r=1} = 1 + \sum_{k=1}^{\infty} \frac{4}{\Pi_k}(\mathrm{Re}(f_k)\cos(k\varphi) - \mathrm{Im}(f_k)\sin(k\varphi)). \tag{22}$$

For illustration purposes, Fig. 2 gives the temperature and heat flux distribution (according to Eq. (21)) for half-sinusoidal heating, i.e.

$$f^*(\varphi) = \begin{cases} \pi\sin(\varphi) - 1 & \varphi \in [0, \pi], \\ -1 & \text{otherwise}, \end{cases}$$

for a selection of parameters. This heating mode corresponds to a pipe heated by radiation from a far-away point source, isolated on the side facing away from the point source.

Some remarks are in order. First, in Eq. (20), the term $r^{|k|}$ is always dominant for increasing r (in both fluid and solid). Hence, high wavenumber contributions are strongly damped the farther away from the outer wall one measures the temperature. This is reminiscent of the St.-Venant principle in solid mechanics, or of the thickness of a Stokes layer depending on the excitation frequency. As a consequence, high k contributions mostly do not travel into the fluid, in particular for thick, well-conducting walls. In general, for solid walls with these properties, the interface heat flux will become increasingly homogeneous, as visualized in Fig. 3. Secondly, the first two terms in Eq. (19) are only present for finite Pe, and they express the total conductive heat flux into the $z < 0$ region: without these terms present, the bulk temperature at $z = 0$ would be zero. Herein, the first term is the contribution of the fluid region (and thus also present in [2]), and the second term is the contribution of the solid region, which vanishes as expected for $\Gamma = 1$ and increases with the solid conductivity (λ_{sf}).

Finally, integrating Eq. (22) over the circumference cancels out all contributions except $k = 0$. In other words, the mean heat transfer (and similarly, the mean Nusselt number) depends only on the mean heat flux, not the way the heat flux is distributed around the circumference. This statement is already implied by [5] ('However, the average temperature difference, computed from the average heat flux, is identical with that predicted for no peripheral flux variation'.), and trivially generalizes to conjugate heat transfer.

2.3. Graetz problem for non-uniform heat flux

In this section, we solve the Graetz problem subject to inhomogeneous heating, which is the limiting case for $\mathrm{Pe} \to \infty$. Axial conduction will be treated in Section 2.4; and we restrict ourselves to the non-conjugated case. The problem is defined by equations Eq. (5), as well as BCs Eq. (6); in particular, Eq. (6b) becomes in absence of a solid:

$$\left.\frac{\partial \theta}{\partial r}\right|_{r=1} = \begin{cases} 1 + f(\varphi) & \text{for } z > 0 \text{ and } \varphi \in [0, 2\pi), \\ 0 & \text{for } z < 0 \text{ and } \varphi \in [0, 2\pi). \end{cases} \tag{23}$$

Again, we formulate the solution as superposition of Fourier modes, i.e. $\theta = \sum_{k=-\infty}^{\infty} \hat{\theta}_k(r, z)\exp(jk\varphi)$. Inserting into Eq. (5), yields

$$\frac{1}{r}\frac{\partial}{\partial r}\left(r\frac{\partial \hat{\theta}_k}{\partial r}\right) - \frac{k^2}{r^2}\hat{\theta}_k + \frac{1}{\mathrm{Pe}^2}\frac{\partial^2 \hat{\theta}_k}{\partial z^2} = u_z \frac{\partial \hat{\theta}_k}{\partial z}. \tag{24}$$

This problem can be rewritten in terms of a linear operator $\mathcal{L}_k$:

$$\frac{\partial \hat{\theta}_k}{\partial z} = \underbrace{\left(\frac{1}{ru_z}\frac{\partial}{\partial r}\left(r\frac{\partial}{\partial r}\right) - \frac{k^2}{r^2 u_z}\right)}_{=:\mathcal{L}_k}\hat{\theta}_k + \frac{1}{\mathrm{Pe}^2 u_z}\frac{\partial^2 \hat{\theta}_k}{\partial z^2}. \tag{25}$$

$\mathcal{L}_k$ is self-adjoint and negative semi-definite (even negative definite for $k \neq 0$) on the space

$$\mathcal{D} := \{\varphi \in H^2((0,1)), \varphi'(1) = 0\} \tag{26}$$

with respect to the inner product

$$\langle u, v\rangle = \int_0^1 uvru_z \mathrm{d}r. \tag{27}$$

These properties are shown in Appendix A. Therefore, for each k there exists an orthogonal basis of $\mathcal{D}$ consisting of eigenfunctions of $\mathcal{L}_k$. To make use of this, we strive to reformulate the problem in such a way that the solution lies within $\mathcal{D}$. To this end, we subtract a function p_k,

$$\tilde{\theta}_k = \hat{\theta}_k - p_k(r,z) \quad \text{where} \quad \frac{\partial p_k}{\partial z} = \mathcal{L}_k(p_k) = \overline{p}_k \equiv \text{const.}, \tag{28}$$

and choose p_k such that it fulfills the boundary condition Eq. (23). Hence, we identify p with the fully developed solution Eqs. (19) and (20) for $z > 0$, and zero for $z < 0$. The constant $\overline{p}_k$ is zero for $k \neq 0$, and 4 for the zeroth mode. In particular, this transformation requires $\tilde{\theta}_k \to 0$ for $z \to \pm\infty$. Eq. (25) then becomes

$$\frac{\partial \tilde{\theta}_k}{\partial z} = \mathcal{L}_k \tilde{\theta}_k + \frac{1}{\mathrm{Pe}^2 u_z} \frac{\partial^2 \tilde{\theta}_k}{\partial z^2}. \tag{29}$$

Initial condition Eq. (6a), boundary condition Eq. (23), and regularity condition Eq. (2b) become, respectively,

$$\lim_{z\to-\infty} \tilde{\theta}_k(r,\varphi,z) \equiv 0 \quad \text{for } r > 0,\ \varphi \in [0, 2\pi) \text{ and all } k \tag{30a}$$

$$\left.\frac{\partial \tilde{\theta}_k}{\partial r}\right|_{r=1} = 0 \tag{30b}$$

$$\left.\frac{\partial \tilde{\theta}_0}{\partial r}\right|_{r=0} = 0; \text{ and } \tilde{\theta}_k(r=0,z) \equiv 0, \text{ for } k \neq 0 \tag{30c}$$

Moreover, since $\hat{\theta}_k$ is continuous at the origin, Eq. (28) imposes a jump condition onto $\tilde{\theta}_k$:

$$\tilde{\theta}_k(r,z)|_{z=0^+} + p_k(r, z=0) = \tilde{\theta}_k(r,z)|_{z=0^-}. \tag{31}$$

For given k, let ϕ_{kj} denote an orthonormal basis of $\mathcal{D}$ consisting of eigenfunctions of the operator $\mathcal{L}_k$, i.e. functions satisfying $\mathcal{L}_k\phi_{kj} = \lambda_{kj}\phi_{kj}$ and $\langle\phi_{kj},\phi_{kj}\rangle = 1$. Here λ_{kj} are the corresponding eigenvalues for the wavenumber k.

Since the transformed solution $\tilde{\theta}_k$ lies in $\mathcal{D}$ – the space where the operator $\mathcal{L}_k$ is self-adjoint – it can be expanded into eigenfunctions:

$$\tilde{\theta}_k = \sum_{j=1}^{\infty} \langle\tilde{\theta}_k,\phi_{kj}\rangle\phi_{kj}, \tag{32}$$

The coefficients $c_{kj}(z) := \langle\tilde{\theta}_k,\phi_{kj}\rangle$ are dependent on z and determined from the system Eqs. (29) and (30). To derive expressions for the coefficients, we take the inner product of Eq. (29) with ϕ_{kj}. Taking the limit $\mathrm{Pe} \to \infty$, we obtain

$$c'_{kj}(z) - \lambda_{kj}c_{kj}(z) = 0 \text{ and thus } c_{kj}(z) = C_{kj}\exp(\lambda_{kj}z). \tag{33}$$

From here on, we will restrict ourselves to the case of $k \neq 0$ to enhance the clarity of the presentation.[2] Following the same steps that lead to (33), we obtain a boundary condition and a jump condition from Eq. (30a) and Eq. (31):

$$\lim_{z\to-\infty} c_{kj}(z) = 0 \tag{34a}$$

$$c_{kj}(0^+) + \langle p|_{z=0^+},\phi_{kj}\rangle = c_{kj}(0^-) \tag{*34b}$$

To simplify Eq. (*34b), we can exploit Eq. (A.1) and Eq. (28) to obtain

$$\langle p|_{z=0^+},\phi_{kj}\rangle = \frac{1}{\lambda_{kj}}\left(\langle\overline{p}_k,\phi_{kj}\rangle - \phi_{kj}(1)\left.\frac{\partial p}{\partial r}\right|_{r=1}\right) = -\frac{\phi_{kj}(1)}{\lambda_{kj}}\left.\frac{\partial p}{\partial r}\right|_{r=1} \tag{*35}$$

The second equality is apparent from $\overline{p}_k = 0$ for $k \neq 0$. For $z < 0$ we immediately see from Eq. (34a) that $\langle\tilde{\theta}_k,\phi_{kj}\rangle = c_{kj} \equiv 0$ due to the operator being negative definite. This was expected because the problem is parabolic for the case $\mathrm{Pe} \to \infty$. For $z > 0$, the integration constant in Eq. (33) becomes

$$C_{kj} = \langle\tilde{\theta}_k,\phi_{kj}\rangle|_{z=0^+} = -\langle p,\phi_{kj}\rangle = \frac{\phi_{kj}(1)}{\lambda_{kj}} f_k \tag{*36}$$

due to Eqs. (28), (23) and (*35).

A Note on the Eigenfunctions. What remains is to determine eigenvalues λ_{kj} and eigenvectors ϕ_{kj}. In general, an analytical expression for the eigenfunctions is not available, however we will sketch how for the case $u_z = 1 - r^2$ this is possible. From the definition of $\mathcal{L}_k$ in Eq. (25), we find that the self-adjoint eigenvalue problem $\mathcal{L}_k\phi_{kj} = \lambda_{kj}\phi_{kj}$ is given by

$$\frac{1}{r}\left(r\phi'_{kj}\right)' - \frac{k^2}{r^2}\phi_{kj} + u_z\mu_{kj}^2\phi_{kj} = 0, \tag{37}$$

where $\lambda_{kj} = -\mu_{kj}^2$. Using the transformation $\phi_{kj}(r) = r^{|k|}\exp(-\eta/2)f(\eta)$, $\eta = \mu_{kj}r^2$, the equation becomes

$$\eta f''(\eta) + (|k| + 1 - \eta)f'(\eta) - \left(-\frac{\mu_{kj}}{4} + \frac{1}{2}(|k|+1)\right) f(\eta) = 0, \tag{38}$$

which is Kummer's equation [15]. Its solution is the confluent hypergeometric function $M(a_{kj}, b_k, \eta)$ where $a_{kj} = -\frac{\mu_{kj}}{4} + \frac{1}{2}(|k|+1)$, $b_k = 1 + |k|$. Therefore, the fundamental solution of Eq. (37) is

$$\phi_{kj}(r) = r^{|k|}\exp(-\frac{\mu_{kj}}{2}r^2)M(a_{kj}, 1+|k|, \mu_{kj}r^2) \tag{39}$$

The eigenvalues are then determined by requiring the boundary condition $\phi'_{kj}(1) = 0$, derived from Eq. (30b), to hold:

$$0 \overset{!}{=} 2M'(a_{kj}, 1+|k|, \mu_{kj}) + \left(\frac{|k|}{\mu_{kj}} - 1\right) M(a_{kj}, 1+|k|, \mu_{kj}). \tag{40}$$

Note that the eigenfunctions and eigenvalues are equal for k and $-k$. Also note that the eigenfunctions trivially fulfill boundary condition Eq. (30c).

The full solution. Using $p(z)$ from Eqs. (19) and (20) for $\mathrm{Pe} = \infty$, i.e.

$$p_k(r) = \begin{cases} 4z - \frac{1}{4}r^4 + r^2 - \frac{7}{24} & k = 0, \\ f_k \frac{r^{|k|}}{|k|} & k \neq 0, \end{cases} \tag{41}$$

we collect the solution θ from Eqs. (8), (28), (32),(33) and (*36), and find

$$\begin{aligned} \theta &= \sum_{k=-\infty}^{\infty} \hat{\theta}_k(r,z)\exp(jk\varphi) \\ &= 4z - \frac{1}{4}r^4 + r^2 - \frac{7}{24} + \sum_{j=2}^{\infty} \frac{\phi_{kj}(1)\exp(\lambda_{kj}z)}{\lambda_{kj}}\phi_{kj} \\ &\quad + \sum_{k=1}^{\infty}\left(\frac{2r^k}{k} + 2\sum_{j=1}^{\infty}\frac{\phi_{kj}(1)\exp(\lambda_{kj}z)}{\lambda_{kj}}\phi_{kj}\right)(\mathrm{Re}(f_k)\cos(k\varphi) \\ &\quad - \mathrm{Im}(f_k)\sin(k\varphi)). \end{aligned} \tag{42}$$

Two modes $\hat{\theta}_1$ and $\hat{\theta}_3$ are displayed exemplarily in Fig. 4, together with a second-order finite differences approximation, the details of which are given in Appendix D. They are in excellent agreement, verifying the analytical solution presented here.

A few remarks follow. Firstly, we observe that the jth eigenvalue of $\mathcal{L}_k$ increases monotonically in k (that is, $\lambda_{1j} < \lambda_{2j} < \cdots$), except for the zero-order mode, where the eigenvalues of $\mathcal{L}_0$ and $\mathcal{L}_2$ coincide (apart from the extra eigenvalue $\lambda_{01} = 0$): $\lambda_{0(j+1)} = \lambda_{2j}$. Therefore, not only do high-order modes in the azimuthal boundary condition decay quickly in the radial direction (see Section 2.2), they also reach the fully developed state much faster than lower-order modes. However, it also means that a mode with period of 2π, if present in the boundary condition, significantly increases the length until a fully developed state is reached. This is an important take-away for the design of systems that are heated only on one side, such as heat pipe solar collectors or concentrated solar power plants. There is an intuitive physical

[2] The $k = 0$ case can be treated in the same framework, but some key simplifications are not possible. We indicate these occurrences with an asterisk in the equation number, and provide their replacements in Appendix C.

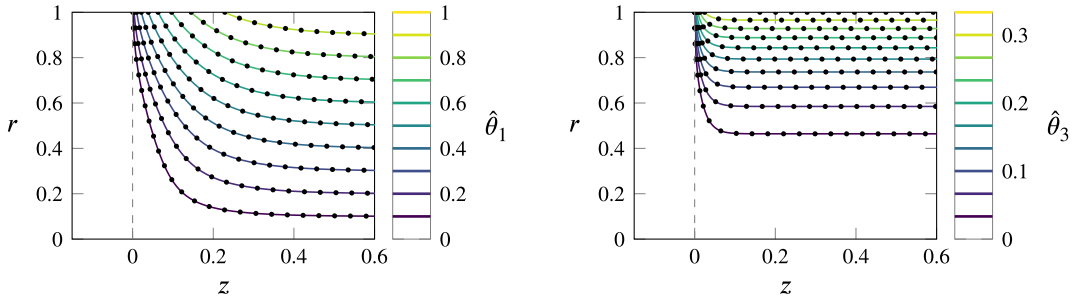

(a) $k = 0$ (b) $k = 3$

Fig. 4. Contour plot of the Fourier modes $\hat{\theta}_k$ for $k = 1$ and $k = 3$, $\mathrm{Pe} \to \infty$. Lines: solution presented herein. Dots: Finite difference approximation for comparison.

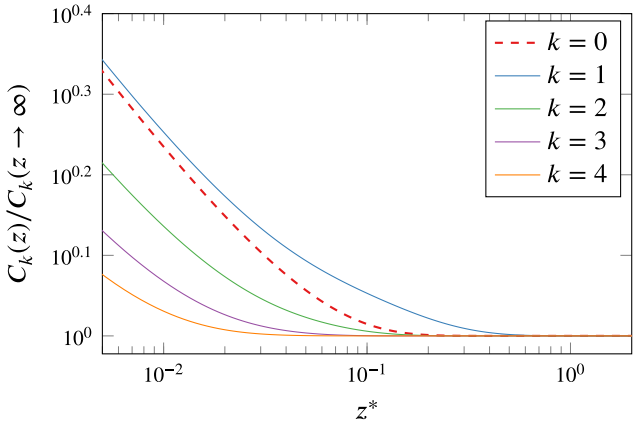

Fig. 5. Diagnostic plot for the thermally fully developed state (see Eq. (43)), different values of k. $k = 0$ is highlighted with dashed linestyle. $\mathrm{Pe} \to \infty$. The ordinate is given in non-dimensional axial length: recall that $z = \mathrm{Pe} R_i z^*$, hence the dimensional thermal entrance length is infinity for $\mathrm{Pe} \to \infty$.

explanation for this behavior: for $k = 0$ and $k = 2$, the information of the changed boundary condition only has to be conducted to the center of the pipe while for $k = 1$, it has to be conducted to the opposite side of the pipe, which takes longer.

In order to graphically evaluate this behavior, we *define* something akin to a Nusselt number for each mode, well knowing that the ordinary definition of the Nusselt number yields zero everywhere for any of the $k > 0$ modes. We define

$$C_k = \frac{-2}{4\int_0^1 \hat{\theta}_k u_z r \mathrm{d}r - \hat{\theta}_k(r=1)} \left.\frac{\partial \hat{\theta}_k}{\partial r}\right|_{r=1}. \tag{43}$$

For $k = 0$, $C_k = \mathrm{Nu}$. For $k > 0$, this quantity does not have an immediate physical interpretation; however the ratio $C_k(z)/C_k(z \to \infty)$ allows us to evaluate how close the radial profile at a given z position is to the fully developed one, hence evaluate thermal entrance lengths for individual modes. This is displayed in Fig. 5. The $k = 1$ mode actually requires significantly longer to reach the fully developed state than a pipe subject to uniform heat flux ($k = 0$). Apart from this, with increasing k, the thermal entrance length decreases.[3]

We also observe that due to Eq. (30c), the eigenfunctions for $k \neq 0$ vanish at the origin, which corresponds to the fact that the temperature at the centerline only depends on the mean of the nonuniform heat flux, not its azimuthal distribution. The statement made at the end of Section 2.2 about the Nusselt number being independent of the heat flux distribution also holds true for the thermal inlet region, as integration over φ always cancels out the last part in Eq. (42).

Secondly, the solution presented here may be extended in various ways. Exchanging the nonuniform heat flux with nonuniform prescribed temperature, we must modify Eq. (28) and the characteristic equation for the eigenvalues, Eq. (40). Similarly, an extension to conjugate heat transfer is possible using the method outlined in [16].

Finally, we note that [10] solves the Graetz problem for a class of non-circular cross sections subject to circumferentially homogeneous boundary condition. The implicitly defined shape $1 - r^2 + \varepsilon r^k \sin(k\varphi) = 0$ defines, for small ε, a closed contour which is $(2\pi)/k$ periodic in r. For $k = 2$, this shape is an ellipse, while for $k \geq 3$ given suitable choice of ε, k-polygons are approximated. For an $\mathcal{O}(\varepsilon)$ approximation, they obtain the same ODE for the eigenfunctions as Eq. (37), and also share the observation that the centerline temperature is independent of $k \geq 1$ modes. We therefore anticipate that the method outlined in Section 2.4 can also be applied to this class of solutions.

2.4. Extended graetz problem for non-uniform heat flux

In this section, we extend the approach taken in Section 2.3 to finite Pe numbers. For clarity of the presentation, we again restrict ourselves to $k \neq 0$ for which the operator $\mathcal{L}_k$ is negative definite; the necessary changes to accommodate the case $k = 0$ are again outlined in Appendix C, and we mark with an asterisk in the main text where such a change would need to be applied. We start with the problem defined by Eqs. (29)–(31). The solution $\tilde{\theta}_k$ still lies in the space $\mathcal{D}$, hence the eigenfunction expansion

$$\tilde{\theta}_k = \sum_{j=1}^{\infty} \langle \tilde{\theta}_k, \phi_{kj} \rangle \phi_{kj}, \tag{44}$$

still holds. For finite Pe, taking the inner product of Eq. (29) with ϕ_{km}, we obtain

$$\frac{\partial}{\partial z}\langle \tilde{\theta}_k, \phi_{km} \rangle = \lambda_{km} \langle \tilde{\theta}_k, \phi_{km} \rangle + \frac{1}{\mathrm{Pe}^2} \sum_{j=1}^{\infty} \frac{\partial^2 \langle \tilde{\theta}_k, \phi_{kj} \rangle}{\partial z^2} \int_0^1 r \phi_{kj} \phi_{km} \mathrm{d}r \tag{45}$$

instead of Eq. (33). This is a system of coupled ODEs. To write it more compactly, we introduce the following names:

$$(c_k)_m := \langle \tilde{\theta}_k, \phi_{km} \rangle, \quad (\Lambda_k)_{jm} := \lambda_{kj} \delta_{jm}, \quad (K_k)_{jm} := \int_0^1 r \phi_{kj} \phi_{km} \mathrm{d}r \tag{46}$$

Note that Λ_k is a negative definite* diagonal matrix and that K_k – being the representation matrix of the scalar product $[u, v] := \int_0^1 u(r) v(r) r \mathrm{d}r$ – is positive definite. Eq. (45) can then be written in matrix form as

$$c_k'(z) = \Lambda_k c_k(z) + \frac{1}{\mathrm{Pe}^2} K_k c_k''(z). \tag{47}$$

[3] For $k = 1$, C_k is within 1% of the fully developed value at $z = 0.392$. This position decays roughly with $k^{-2.1 \pm 0.2}$.

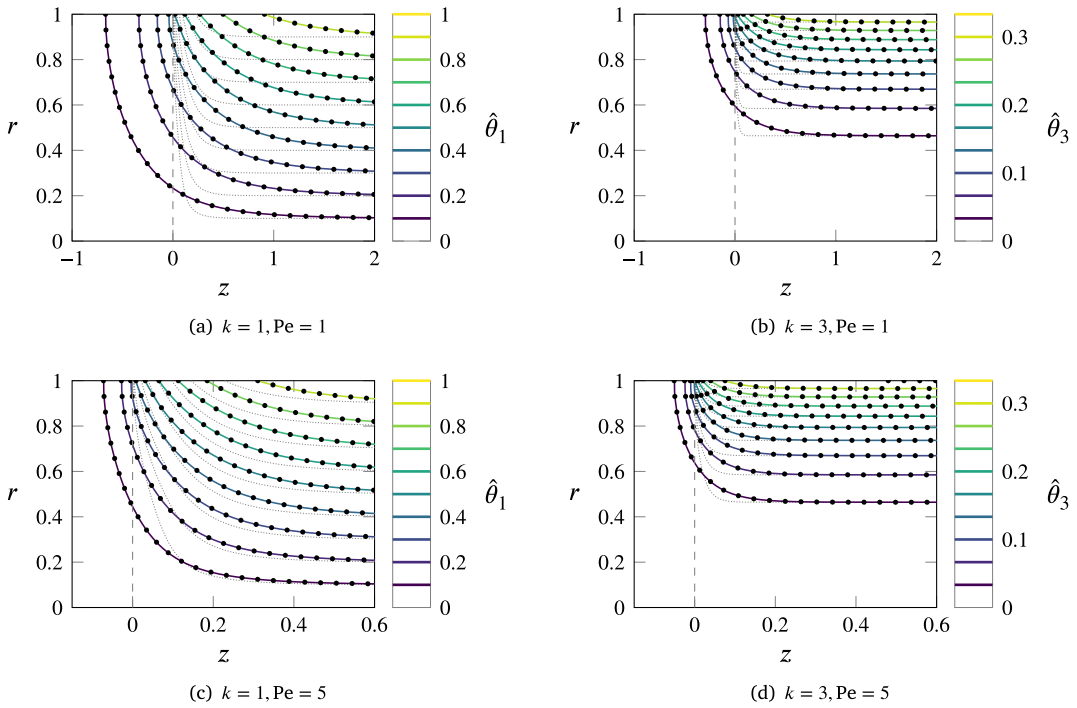

(a) $k = 1, \mathrm{Pe} = 1$ (b) $k = 3, \mathrm{Pe} = 1$

(c) $k = 1, \mathrm{Pe} = 5$ (d) $k = 3, \mathrm{Pe} = 5$

Fig. 6. Contour plot of the Fourier modes $\hat{\theta}_k$ for $k = 1$ (left) and $k = 3$ (right) for $\mathrm{Pe} = 1$ (top) and $\mathrm{Pe} = 5$ (bottom). Lines: solution of Section 2.4. Dots: Finite difference approximation for comparison. The $\mathrm{Pe} \to \infty$ solution is indicated with thin dashed lines.

As Eq. (47) is a second order linear differential equation, it has two linearly independent solutions. In the limit $\mathrm{Pe} \to \infty$, Eq. (47) becomes first order and hence there will be only one solution — the one derived in Section 2.3. Inserting the ansatz

$$c_k = \exp(A_k z) c_{k0} \tag{*48}$$

into Eq. (47) leads to the characteristic equation

$$A_k = \Lambda_k + \frac{1}{\mathrm{Pe}^2} K_k A_k^2. \tag{49}$$

In Appendix B, we prove that this quadratic matrix equation always has one solution with only positive and one solution with only negative eigenvalues (*), which we label with A_k^+ and A_k^- respectively and which depend on Pe. A method for constructing those solutions is also given in Appendix B. Denoting the r.h.s. of Eq. (*35) as q_k, Eqs. (34a) and (*35) yield

$$c_k(z) = \begin{cases} \exp(A_k^+ z) c_{k0} & \text{for } z < 0, \\ \exp(A_k^- z)(c_{k0} - q_k) & \text{for } z > 0. \end{cases} \tag{50}$$

Requiring the solution to be C^1 at the origin yields a linear equation system for the coefficient c_{k0}:

$$A_k^+ c_{k0} = A_k^-(c_{k0} - q_k) \quad \to \quad (A_k^+ - A_k^-) c_{k0} = -A_k^- q_k. \tag{*51}$$

The solution is assembled from Eqs. (8), (19), (20), (28), (44), (*48) and (50) as

$$\theta = \begin{cases} c_0(z) \cdot \boldsymbol{\Phi}_0 + \sum_{k=1}^{\infty} c_k(z) \cdot \boldsymbol{\Phi}_k (\mathrm{Re}(f_k) \cos(k\varphi) - \mathrm{Im}(f_k) \sin(k\varphi)) & \text{if } z \le 0, \\ 4z - \frac{1}{4} r^4 + r^2 - \frac{7}{24} + \frac{8}{\mathrm{Pe}^2} + c_0(z) \cdot \boldsymbol{\Phi}_0 & \\ \quad + \sum_{k=1}^{\infty} 2 \left(\frac{r^k}{k} + c_k(z) \cdot \boldsymbol{\Phi}_k \right) (\mathrm{Re}(f_k) \cos(k\varphi) - \mathrm{Im}(f_k) \sin(k\varphi)) & \text{if } z > 0, \end{cases} \tag{52}$$

where $\boldsymbol{\Phi}_k := (\phi_{k1}, \phi_{k2}, \ldots)$ denotes the vector of eigenfunctions corresponding to $\mathcal{L}_k$.

r-z contours of two modes $\hat{\theta}_1$ and $\hat{\theta}_3$ are displayed for two different Pe numbers in Fig. 6. For verification of the analytical solution, we additionally show a corresponding numerical solution, the details of which are given in Appendix D. Both are in excellent agreement. As is known for $k = 0$ [2], reducing the Pe number increases the length (using the non-dimensionalization $z = \mathrm{Pe} R_i z^*$) until which the change in boundary condition is transmitted upstream as well as the thermal development length. The latter effect is stronger for $k \neq 0$ than for the homogeneous case, and appears to affect modes corresponding to higher k stronger. This can also can be seen from Fig. 8. As a result, to accurately resolve the temperature field in the vicinity of $z = 0$, a larger number of azimuthal modes is required for decreasing Pe.

Fig. 7 shows the thermal entrance behavior of a pipe with half-sinusoidal heating, at two different Pe numbers already discussed above. The centerline temperature reaches the fully developed state relatively quick (after 0.2 resp. 1 axial units),[4] while the temperature at the top and bottom takes significantly longer to develop (0.4 resp. 3 axial units). Of course, both Pe numbers lead to the same fully-developed state after subtraction of the (z-dependent) bulk temperature.

Finally, we display the thermal entrance length depending on Pe in Fig. 9. It is crucial to remember that z was non-dimensionalized with $\mathrm{Pe} R_i$. If axial conduction is neglected (or negligible), the thermal entrance length (when dimensionalized with the pipe radius or diameter) therefore increases linearly with Pe. Considering axial conduction

[4] For $\mathrm{Pe} = 1$, $z = R_i z^*$. Therefore these development lengths can be read as the streamwise coordinate normalized with the radius. The $\mathrm{Pe} \to \infty$ case should be considered only in a limiting sense: the solution also takes infinitely long to develop. Rather, it shows which error is made by neglecting axial conduction for finite Pe numbers.

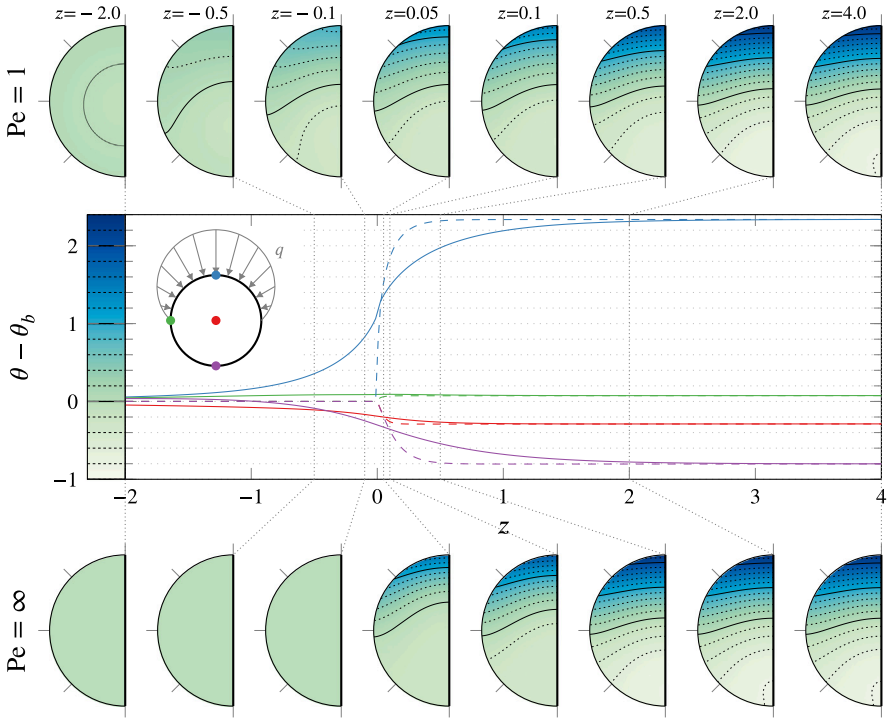

Fig. 7. Dimensionless temperature distribution for half-sinusoidal heating in the thermal entrance region. The main plot displays the temperature at four distinct locations (centerline, top, bottom, side) over the axial coordinate, for two different Pe numbers: Pe = ∞ (dashed lines) and Pe = 1 (solid lines). At indicated locations, the dimensionless temperature distribution in the pipe is plotted. The thermal entrance of the overall Nu number behaves as the centerline temperature (red). (For interpretation of the references to color in this figure legend, the reader is referred to the web version of this article.)

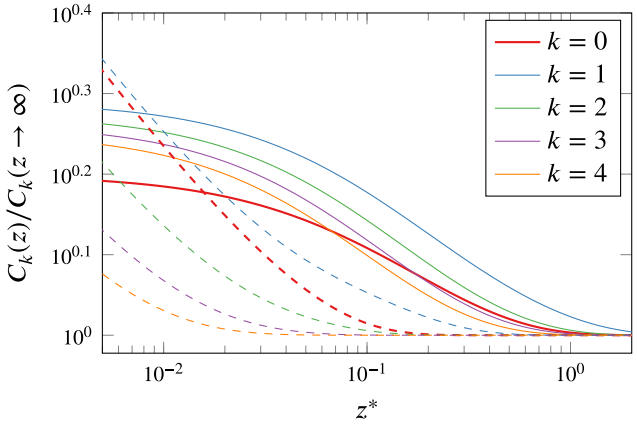

Fig. 8. Diagnostic plot for the fully developed state (see Eq. (43)), different values of k. $k = 0$ is highlighted with dashed linestyle. $Pe = 1$ (solid lines). Pe → ∞ (dashed) from Fig. 5 added for reference.

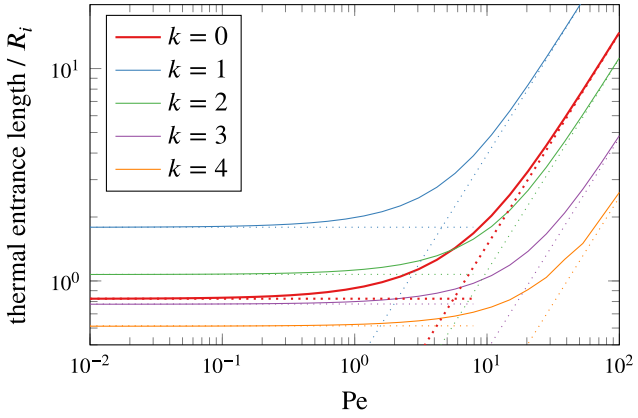

Fig. 9. Thermal entrance length (defined as the position where $C_k(z)$ deviates 1% from $C_k(z \to \infty)$) for different values of k. Solid lines: including axial conduction. Dotted lines: neglecting axial conduction (right) / axial convection (left).

becomes relevant for low Pe, where the solution will ultimately become independent of Pe. This can be seen by non-dimensionalizing z with R_i instead, leading to

$$\frac{1}{r}\frac{\partial}{\partial r}\left(r\frac{\partial \hat{\theta}_f}{\partial r}\right) - \frac{k^2}{r^2}\hat{\theta}_f + \frac{\partial^2 \hat{\theta}_f}{\partial z^2} = \mathrm{Pe} u_z \frac{\partial \hat{\theta}_f}{\partial z}. \tag{53}$$

For Pe → 0, the convection term is negligible and the problem becomes a purely diffusive one (note that for small, but nonzero Pe the 'outlet condition' – i.e. the fully developed solution for $z \to \infty$ – for $k = 0$ still contains u_z). Hence, the solution becomes independent of Pe, and so does the thermal entrance length when made dimensionless with the pipe radius. Similarly to Section 2.3, the limiting solution for Pe → 0 is straightforward to derive, as the PDE again gives rise to a (different) self-adjoint operator whose eigenfunctions are the Bessel functions of the first kind J_k. As visible from Fig. 9, the solution for finite Pe indeed follows nicely both limits for Pe → ∞ and Pe → 0.

3. Conclusion

We have derived novel analytical solutions for a variety of problems related to azimuthally nonuniform heating of a laminar pipe flow. All

solutions rely on the separation into azimuthal modes. Starting from the case of thermally fully developed flow in a thick-walled pipe subject to inhomogeneous heating, we demonstrated that azimuthal variations in the prescribed heat flux only yield small changes far away from the source of the variation, a result similar to St-Venant's principle in solid mechanics. As a further key result, the (dimensionless) centerline temperature and global Nusselt number only depend on the $k = 0$ mode, and not how the heating is distributed around the circumference.

Next, we have derived the solution to the regular Graetz problem for this configuration, i.e. the thermal entrance behavior for $\mathrm{Pe} \to \infty$ in a nonuniformly heated pipe. After obtaining the PDE for each mode and proving the selfadjointness of its differential operator, the solution is expressed as eigenfunction expansion of said operator and the coefficients determined.

Following what we observed for the fully developed region, we note that not only do high-k contributions in the heat flux decay quickly towards the bulk of the pipe, they also reach the fully-developed state much faster, with the remarkable exception of $k = 1$. Mathematically speaking, $k = 1$ has the lowest non-zero eigenvalue of all $\mathcal{L}_k$. The presence of such a mode can delay the onset of the fully-developed state significantly.

Trivially, the above statement about Nusselt number and centerline temperature being independent of $k \neq 0$ modes generalizes to the thermal entrance region.

Finally, we have derived an extension of the above solution for finite Pe numbers, i.e. the *extended* Graetz problem. Unlike in the $\mathrm{Pe} \to \infty$ case or $k = 0$ [2], the operator describing the behavior for $k \neq 0, \mathrm{Pe} \ll \infty$ is nonselfadjoint and an expansion in terms of orthogonal eigenfunctions seems out of reach. Instead, we employ the eigenbasis derived in the previous section again — thereby transforming the problem into an infinite system of coupled ODEs. As far as the authors are aware, this approach has not been used to tackle the extended Graetz problem. We show that the eigenfunction coefficients are well-behaved for both $z \to -\infty$ and $z \to \infty$, and have cross-compared the solution against a finite-difference implementation of the problem.

Decreasing the Pe number disproportionally affects the $k \neq 0$ modes; while the length of the thermal entrance region (expressed in $z^* = z/(R\mathrm{Pe})$) is known to increase in the homogeneous case when including axial conduction instead of neglecting it, nonzero azimuthal modes are affected more strongly.

Some of the research presented here may hold valuable insights for turbulent pipe flow as well. [17] showed that for two Prandtl numbers and various Reynolds numbers, the azimuthal heat flux distribution did not affect the Nusselt number. In the laminar case, this observation follows trivially after separation of the PDE, which is not possible for turbulent flow. Furthermore, little data exists for the thermal entrance behavior of turbulent flow. Based on the solution of the laminar Graetz problem, we expect that pointwise first-order statistics of the temperature has a longer thermal development length compared to the global Nusselt number. As the production of temperature variance depends on the gradient of temperature, we expect that such second-order statistics require an even longer development region.

In addition to the extension into the turbulent regime, future research may also employ the presented formalism for the solution of the laminar Graetz problem for other cases of inhomogeneous boundary conditions, such as conjugate heat transfer, nonuniform prescribed temperature or non-circular geometries.

CRediT authorship contribution statement

Jonathan Neuhauser: Writing – review & editing, Writing – original draft, Visualization, Validation, Software, Methodology, Investigation, Formal analysis, Data curation, Conceptualization. **Jan-Henrik Metsch:** Writing – review & editing, Writing – original draft, Investigation, Formal analysis, Conceptualization. **Davide Gatti:** Supervision, Funding acquisition, Conceptualization. **Bettina Frohnapfel:** Writing – review & editing, Supervision, Funding acquisition.

Declaration of competing interest

The authors declare that they have no known competing financial interests or personal relationships that could have appeared to influence the work reported in this paper.

Acknowledgments

We greatly acknowledge the support by the German Research Foundation (DFG) under research project 423710075. We further thank L. Bürk for the initial implementation of the homogeneous reference solution and W. Reichel for helpful discussions.

Appendix A. Properties of $\mathcal{L}_k$

Let $\mathcal{D} := \{\varphi \in H^2((0,1)), \varphi'(1) = 0\}$. Here, the boundary condition is to be understood in the sense of the Sobolev trace. We equip $\mathcal{D}$ with the inner product defined by Eq. (27). Then, for all k, the operator $\mathcal{L}_k$ is self-adjoint on $\mathcal{D}$ as can be shown by means of partial integration, i.e.

$$\begin{aligned}\langle \mathcal{L}_k u, v\rangle - \langle u, \mathcal{L}_k v\rangle &= \int_0^1 (ru')'v - \frac{k^2}{r}uv - (rv')'u + \frac{k^2}{r}uv\,\mathrm{d}r \\ &= \int_0^1 (ru')'v - (rv')'u\,\mathrm{d}r \\ &= \left[(ru')v - (rv')u\right]_0^1 - \int_0^1 (ru')v' - (rv')u'\,\mathrm{d}r \\ &= u'(1)v(1) - v'(1)u(1) \\ &= 0.\end{aligned} \tag{A.1}$$

Moreover, for $k \neq 0$, the operator is negative definite, since

$$\begin{aligned}\langle \mathcal{L}_k u, u\rangle &= \int_0^1 (ru')'u - \frac{k^2}{r}u^2\,\mathrm{d}r \\ &= \left[ru'u\right]_0^1 - \int_0^1 r(u')^2 - \int_0^1 \frac{k^2}{r}u^2\,\mathrm{d}r \\ &= -\int_0^1 r(u')^2 + \frac{k^2}{r}u^2\,\mathrm{d}r.\end{aligned} \tag{A.2}$$

For $k \neq 0$, this expression is strictly negative unless $u \equiv 0$. In particular, all eigenvalues must be negative. For $k = 0$, the function $\phi \equiv 2$ is a (normalized) eigenvector corresponding to $\lambda = 0$. Hence, the operator is only negative semi-definite.

Appendix B. Solution of the linear second-order system for the extended Graetz problem

To motivate the analysis, we first discuss a scalar version of the matrix equation (49), which can be understood as truncating the eigenfunction expansion after the first term:

$$\mu = \lambda + \frac{\kappa}{\mathrm{Pe}^2}\mu^2 \qquad \text{with } \lambda < 0 \text{ and } \kappa, \mathrm{Pe} > 0. \tag{B.1}$$

In this easy example, the solution can be derived from the quadratic formula

$$\mu = \frac{(\mathrm{Pe} \pm \sqrt{\mathrm{Pe}^2 - 4\lambda\kappa})\mathrm{Pe}}{2\kappa}. \tag{B.2}$$

Since $\lambda < 0$ and $\kappa, p > 0$, taking '−' yields a negative and taking '+' yields a positive solution (which becomes singular for $\mathrm{Pe} \to \infty$, which corresponds to equation (B.1) becoming first order). This motivates the formulation of the following theorem:

Theorem B.1. *Let $A, B, C \in \mathbb{R}^{n\times n}$ be symmetric, positive definite matrices. Then the matrix equation*

$$AX^2 - BX - C = 0 \tag{B.3}$$

has a solution with only positive eigenvalues and a solution with only negative eigenvalues.

Eq. (B.3) is the characteristic equation for the following second-order ODE system

$$A\ddot{x} - B\dot{x} - Cx = 0, \quad x \in C^\infty(\mathbb{R}, \mathbb{R}^{n\times n}) \tag{B.4}$$

which can be rewritten into a first-order system like

$$\frac{\mathrm{d}}{\mathrm{d}t}\begin{bmatrix} x \\ \dot{x}\end{bmatrix} = \underbrace{\begin{bmatrix} 0 & I \\ A^{-1}C & A^{-1}B\end{bmatrix}}_{=:M}\begin{bmatrix} x \\ \dot{x}\end{bmatrix} \tag{B.5}$$

with solution $[x(t), \dot{x}(t)]^\top = \exp(tM)[x(0), \dot{x}(0)]^\top$. For simplicity of the presentation, let us assume that M is diagonalizable; if this is not the case, a similar construction can be based on the Jordan form. We then have a matrix L such that

$$L^{-1}ML = \mathrm{diag}(m_1, \dots, m_{2n}) =: D \tag{B.6}$$

ODE Eq. (B.5) is then rewritten as

$$\frac{\mathrm{d}}{\mathrm{d}t}\left(L^{-1}\begin{bmatrix} x \\ \dot{x}\end{bmatrix}\right) = L^{-1}ML\left(L^{-1}\begin{bmatrix} x \\ \dot{x}\end{bmatrix}\right). \tag{B.7}$$

Defining $L^{-1}\left[x, \dot{x}\right]^\top =: q$, we deduce that $q(t) = \mathrm{diag}(\exp(m_1 t), \dots, \exp(m_{2n}t))q(0)$. Thus, we extract x as

$$x(t) = (Lq(t))_1 = \left(\begin{bmatrix} L_{11} & L_{12} \\ L_{21} & L_{22}\end{bmatrix}\begin{bmatrix} \exp(tD_{11})q(0)_1 \\ \exp(tD_{22})q(0)_2\end{bmatrix}\right)_1 \tag{B.8}$$

The indices here are block matrix indices. We choose $q(0)_2 = 0$ and find $x(0) = L_{11}q(0)_1$, $\dot{x} = L_{11}D_{11}q(0)_1$ and $\ddot{x}(0) = L_{11}D_{11}^2 q(0)_1$. Inserting into the ODE Eq. (B.4) gives (exploiting that $q(0)_1$ can be freely chosen)

$$AL_{11}D_{11}^2 - BL_{11}D_{11} - CL_{11} = 0, \tag{B.9}$$

and after right-multiplying L_{11}^{-1}, we find

$$A(L_{11}D_{11}L_{11}^{-1})^2 - B(L_{11}D_{11}L_{11}^{-1}) - C = 0. \tag{B.10}$$

$L_{11}D_{11}L_{11}^{-1}$ is therefore a solution of Eq. (B.3) with eigenvalues $m_1, \dots, m_n$. However, we can order the eigenvalues in Eq. (B.6) arbitrarily by reordering the columns of L. Hence, by ordering the eigenvalues accordingly, we can produce a solution with an arbitrary choice of n of the eigenvalues of M.

Therefore, the proof of Theorem B.1 reduces to proving that M has n positive and negative eigenvalues, which is done in the following section. For $\alpha \in [0, 1]$ we define the matrix

$$M_\alpha = \begin{bmatrix} 0 & I \\ A^{-1}C & \alpha A^{-1}B\end{bmatrix}. \tag{B.11}$$

For $\alpha = 1$ we obtain the original matrix M. Let us define

$$n^\pm(\alpha) := \#\text{purely real } (+)/(-) \text{ eigenvalues of } M_\alpha \tag{B.12}$$

For $\alpha = 0$, the matrix simplifies considerably; we can compute the eigenvalues easily and see that $n^+(0) = n^-(0) = n$. The idea is to follow the eigenvalues as α increases. This is justified by the well-known fact that the solutions of a polynomial depend continuously on the coefficients. To ensure that $n^+(\alpha) = n^-(\alpha)$ remains true along this homotopy, we follow these steps:

1. Prove that all eigenvalues of M_α are real
2. Prove that the eigenvalues are either strictly negative or have a positive lower bound for $\alpha \neq 0$
3. The eigenvalues remain bounded along the homotopy and can therefore not diverge
4. Use that for M_0, $n^\pm(0) = n$ to conclude the proof of Theorem B.1.

Lemma 1. *0 is not an eigenvalue of M_α.*

Proof. The proof is by contradiction. Supposing the opposite, there exists nonzero $c_0 = [c_1, c_2]^\top \in \mathbb{C}^{2n}$ such that $M_\alpha c_0 = 0$. Then $c_2 = 0$ and $A^{-1}Cc_1 = 0$. Multiplying by A and then by c_1^*, we find $c_1^* \cdot Cc_1 = 0$. This is a contradiction. Indeed, since C is positive definite, $c_1^* \cdot Cc_1 = 0$ implies $c_1 = 0$ and hence $c_0 = [c_1, c_2]^T = 0$. □

For the following lemma, let

$$\|A\| := \sup_{v\in\mathbb{R}^n, \|v\|=1} \|Av\| \quad \text{and} \quad m(B) := \inf_{v\in\mathbb{R}^n, \|v\|=1} v \cdot Bv$$

Since B is a positive definite matrix, $m(B)$ is simply the smallest eigenvalue of B and in particular positive.

Lemma 2. *The eigenvalues of M_α are real. Furthermore, every eigenvalue of M_α satisfies one of the following:*

$$\lambda < 0 \quad \text{or} \quad \lambda \geq \alpha\frac{m(B)}{\|A\|}$$

Finally, for M_0, $n^+(0) = n^-(0) = n$.

Proof. Let λ be an eigenvalue of M_α and let $c_0 = [c_1, c_2]^T \in \mathbb{C}^{2n}$ be a nonzero eigenvector, i.e. $M_\alpha c = \lambda c$. Then

$$\lambda\begin{bmatrix} c_1 \\ c_2\end{bmatrix} = \begin{bmatrix} 0 & I \\ A^{-1}C & \alpha A^{-1}B\end{bmatrix}\begin{bmatrix} c_1 \\ c_2\end{bmatrix} = \begin{bmatrix} c_2 \\ A^{-1}Cc_1 + \alpha A^{-1}Bc_2\end{bmatrix}$$

The first component reads $c_2 = \lambda c_1$. From Lemma 1, we know that $\lambda \neq 0$ and hence $c_2 \neq 0$ as otherwise $c = 0$. Inserting the first into the second component, we get

$$\lambda^2 c_2 = A^{-1}Cc_2 + \alpha A^{-1}B\lambda c_2$$

Multiplying with A and then subsequently with c_2^*, we get, after rearranging the quadratic equation

$$\lambda^2 = \frac{c_2^* \cdot Cc_2}{c_2^* \cdot Ac_2} + \alpha\frac{c_2^* \cdot Bc_2}{c_2^* \cdot Ac_2}\lambda$$

Defining

$$p := \alpha\frac{c_2^* \cdot Bc_2}{c_2^* \cdot Ac_2} \quad \text{and} \quad q := \frac{c_2^* \cdot Cc_2}{c_2^* \cdot Ac_2}$$

Then $p \geq 0$ ($p = 0$ only when $\alpha = 0$) and $q > 0$ due to the properties of A, B and C. By these definitions, $\lambda^2 = p\lambda + q$, and hence

$$\lambda = \frac{p}{2} \pm \sqrt{\frac{p^2}{4} + q}. \tag{B.13}$$

The radicand is positive, and thus λ is real. Furthermore, the claimed bounds for λ follow directly from Eq. (B.13). Indeed, taking the negative sign shows $\lambda < 0$ while taking the positive sign yields $\lambda \geq p$.

Finally, for $\alpha = 0$, we show that $n^+(0) = n^-(0)$. To this end, consider the map $\sigma(c_1, c_2, \lambda) = (-c_1, c_2, -\lambda)$. Clearly $\sigma^2 = \mathrm{id}$ and an easy computation shows that σ maps an eigenvector-eigenvalue pair to another such pair — importantly with an eigenvalue with the opposite sign. By virtue of σ each positive eigenvalue has a negative partner and vice versa. Hence $n^+(0) = n^-(0)$. □

Lemma 3. *The eigenvalues of M_α are uniformly bounded over α.*

Proof. For each eigenvalue, either $|\lambda| \leq 1$ or $|\lambda| > 1$. In the first case we already have a bound. In the second case, we consider the characteristic polynomial

$$0 = \det\left(\lambda I - M_\alpha\right) = \det\left(\begin{bmatrix} \lambda I & -I \\ -A^{-1}C & \lambda I - \alpha A^{-1}B\end{bmatrix}\right) = \sum_{k=0}^{2n} c_k(\alpha, A, B, C)\lambda^k.$$

Since the coefficients c_k are mere polynomials in the entries of A^{-1}, B, C and in α, they are all bounded uniformly over α. Moreover, $c_{2n} = 1$. Dividing by λ^{2n-1} yields by means of the triangle inequality,

$$|\lambda| \le \sum_{k=0}^{2n-1} |c_k||\lambda|^{k-2n-1} \le \sum_{k=0}^{2n-1} |c_k|$$

where in the last step, we have used $|\lambda| > 1$. Therefore, we have established a uniform bound for all eigenvalues of M_α independent of α. □

To summarize: By Lemma 2, eigenvalues are real. By Lemma 1, eigenvalues cannot cross 0 and by Lemma 3, they cannot diverge. Thus, the number of positive/negative eigenvalues counted with multiplicity remains constant along the homotopy $[0,1] \ni \alpha \mapsto M_\alpha \in \mathbb{R}^{n\times n}$. In other words $n^+(\alpha) = n^-(\alpha) = n$ for all $\alpha \in [0,1]$. This proves Theorem B.1.

Finally, we extend Theorem B.1 to the slightly more general case where C is only positive semi-definite. In the introductory toy problem, this corresponds to allowing the edge case $\lambda = 0$. We then find two solutions: $\mu = 0$ and $\mu = \frac{p^2}{\kappa}$. The following corollary shows that this intuition carries over to the matrix setting.

Corollary 1. *Let $A, B, C \in \mathbb{R}^{n\times n}$ be symmetric matrices, A and B positive definite and C positive semi-definite. Then the matrix equation*

$$AX^2 - BX - C = 0 \tag{B.14}$$

has a solution with only positive eigenvalues and a solution with only nonpositive eigenvalues.

Proof. If C is positive definite, then the statement is proven in Theorem B.1. Otherwise, let $C_\varepsilon = C + \varepsilon I$. Then for all $\varepsilon > 0$ Theorem B.1 implies that the equation

$$AX^2 - BX - C_\varepsilon = 0$$

has a solution with only positive and one solution with only negative eigenvalues. By Lemma 2, the positive eigenvalues of the first solution are actually bounded by $\lambda \ge \frac{m(B)}{\|A\|} > 0$ from below, independent of ε. Following a homotopy argument as before, this bound extends to $\varepsilon = 0$, while the upper bound of the nonpositive eigenvalues becomes $\lambda \le 0$. Therefore, the number of positive eigenvalues must remain constant along ε. □

Appendix C. Modification of the solution for $k = 0$

The procedure outlined in Sections 2.3 and 2.4 requires a few modifications for the $k = 0$ case, as some simplifications no longer hold.

Modifications to the solution of the regular graetz problem for $k = 0$. First, the jump condition Eq. (*35) is evaluated directly:

$$\langle p|_{z=0^+}, \phi_{01}\rangle = \langle p|_{z=0^+}, 2\rangle = \frac{4}{\mathrm{Pe}^2} = q_{01}, \tag{C.1}$$

which vanishes for $\mathrm{Pe} \to \infty$. From Eqs. (33) and (34a), we see that the coefficient corresponding to the constant eigenfunction must vanish for all z. For all other eigenfunctions of $\mathcal{L}_0$, the coefficient given by Eq. (*36) is unchanged.

Modifications to the solution of the extended graetz problem for $k = 0$. For the extended Graetz problem, the matrix form (Eq. (49)) is unchanged. However, Λ_0 is only negative semi-definite. Following Corollary 1, A_0^+ will still be positive definite, while A_0^- becomes negative semi-definite. Therefore, the matrix exponential is still 'well-behaved' towards both $z \to \pm\infty$.

In case of $k = 0$, $\frac{\partial p}{\partial z}$ changes across $z = 0$, and this change must be reflected in the coefficients. Hence,

$$\left.\frac{\partial\langle\tilde\theta_0, \phi_{0j}\rangle}{\partial z}\right|_{z=0^+} + \langle\frac{\partial p}{\partial z}, \phi_{0j}\rangle = \left.\frac{\partial\langle\tilde\theta_0, \phi_{0j}\rangle}{\partial z}\right|_{z=0^-} \tag{*C.2}$$

where $\frac{\partial p}{\partial z}$ is a constant in r and hence $d_j = \langle\frac{\partial p}{\partial z}, \phi_{0j}\rangle$ vanishes except for the constant eigenfunction. Here we find $d_j = \delta_{1j}\int_0^1 8(1-r^2)r\mathrm{d}r = 2\delta_{1j}$. Finally,

$$c_0(z) = \begin{cases} \exp(A_0^+ z)c_{00} & \text{for } z < 0, \\ \exp(A_0^- z)(c_{00} - q_0) & \text{for } z > 0. \end{cases} \tag{*C.3}$$

c_{00} is determined from Eq. (*C.2), i.e. $A_0^+ c_{00} = A_0^-(c_{00} - q_0) + d$, that is $(A_0^+ - A_0^-)c_{00} = d - A_0^- q_0$.

Verification. Figure Fig. C.10 compares the solution obtained in this way with the reference solution from [2] for two different Péclét numbers, and they are in excellent agreement. From a computational efficiency standpoint, the solution established here has certain advantages over the literature solution. The most expensive operation is the computation of eigenvalues, and accurate evaluation of the eigenfunctions. For this solution, they are independent of Pe and hence only have to be computed once for each k. Furthermore, the more computationally expensive complex arithmetic required to determine the positive eigenvalues in [2] is not needed. That being said, computational effort to evaluate any of those solutions is insignificant by today's standards.

Appendix D. Description of the finite difference approximation

Figs. 4 and 6 display a finite difference approximation of the solution to Eq. (24), in order to cross-check the analytical solution presented herein. To obtain the aforementioned figures, we consider Eq. (24) subject to boundary conditions

$$\lim_{z\to-\infty} \hat\theta_k(r,\varphi,z) \equiv 0 \quad \text{for } r > 0,\ \varphi \in [0,2\pi) \text{ and all } k \tag{D.1}$$

$$\left.\frac{\partial\hat\theta_k}{\partial r}\right|_{r=1} = \begin{cases} 0 & \text{for} z < 0 \\ 1 & \text{for} z \ge 0 \end{cases} \quad \text{for } \varphi \in [0,2\pi) \text{ and all } k \tag{D.2}$$

$$\left.\frac{\partial\hat\theta_0}{\partial r}\right|_{r=0} = 0; \text{ and } \tilde\theta_k(r=0,z) \equiv 0, \text{ for } k \ne 0 \tag{D.3}$$

which are the BCs from Eq. (30), but without the transformation Eq. (28). The problem is discretized on an equidistant cartesian grid of $n_r \times n_z = 800 \times 500$ points in radial and axial direction, respectively. The domain size in axial direction is twice the range of the z axis in Figs. 4 and 6.

All spatial derivatives in Eq. (24) are discretized with second-order finite differences. The forcing term $u_z(r)$ is prescribed analytically. The boundary conditions (Dirichlet at the inlet, Neumann ($k = 0$) / Dirichlet ($k \ne 0$) at $r = 0$, Neumann at $r = 1$, and zero second derivative at the outlet to account for the linear increase in $\hat\theta$ for $k = 0$) are discretized with first-order finite differences, except for the $r = 1$ boundary condition, where significant curvatures in radial direction are expected. The solution is then obtained by inverting the resulting linear equation system directly.

Doubling the spatial resolution in both directions leads to a maximum pointwise deviation of less than 0.01 in all displayed cases; the highest deviations are found near the discontinuity of the boundary condition, i.e. $r = 1, z = 0$. The grid is therefore sufficiently fine in order to resolve the details of the temperature mode, allowing for a meaningful comparison with the analytical result.

The numerical code is included in the auxiliary material [18].

Data availability

The Python package including all code to re-create the Paper's figures has been published on https://github.com/joneuhauser/graetz/ [18].

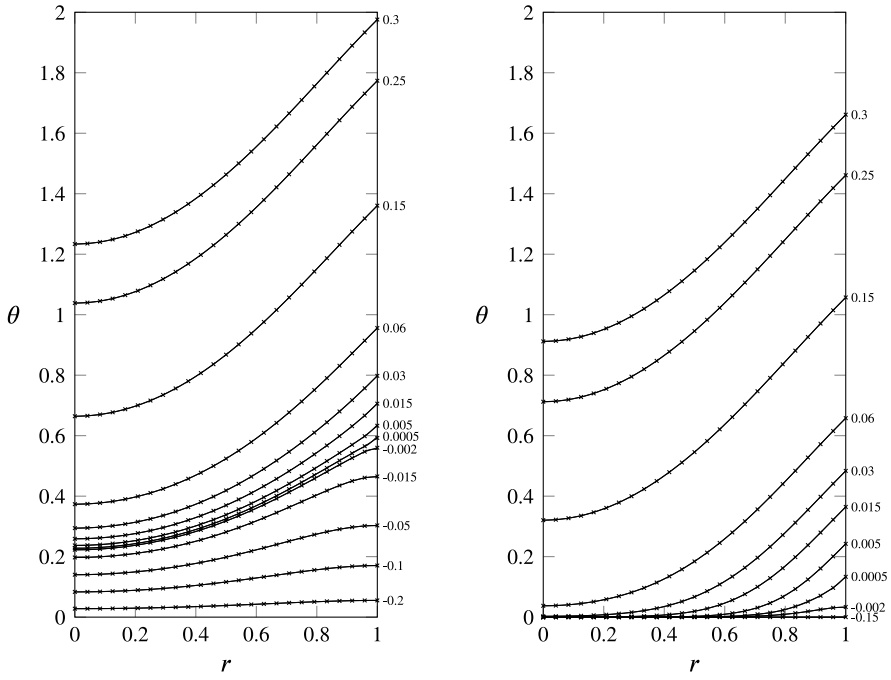

(a) Pe = 5 (b) Pe = 50

Fig. C.10. Dimensionless temperature profiles for the extended Graetz problem with homogeneous Neumann boundary conditions for various z locations (indicated to the right of the lines) and two different Pe numbers. Markers: Reference solution by [2], Lines: $k = 0$ solution presented in Section 2.4 and Appendix C.

References

[1] L. Graetz, Über die Wärmeleitungsfähigkeit von Flüssigkeiten, Erste Abhandlung, Ann. Phys., Lpz. 254 (1) (1882) 79–94, http://dx.doi.org/10.1002/andp.18822540106.

[2] E. Papoutsakis, D. Ramkrishna, H.C. Lim, The extended Graetz problem with prescribed wall flux, AIChE J. 26 (5) (1980) 779–787, http://dx.doi.org/10.1002/aic.690260511.

[3] E. Papoutsakis, D. Ramkrishna, H.C. Lim, The extended Graetz problem with Dirichlet wall boundary conditions, Appl. Sci. Res. 36 (1) (1980) 13, http://dx.doi.org/10.1007/BF00420067.

[4] J. Newman, Extension of the Lévêque Solution, J. Heat Transf. 91 (1) (1969) 177–178, http://dx.doi.org/10.1115/1.3580091.

[5] W. Reynolds, Turbulent heat transfer in a circular tube with variable circumferential heat flux, Int. J. Heat Mass Transfer 6 (6) (1963) 445–454, http://dx.doi.org/10.1016/0017-9310(63)90119-4.

[6] B. Gatewood, XXIII. Thermal stresses in long cylindrical bodies, Lond. Edinb. Dublin Philos. Mag. J. Sci. 32 (213) (1941) 282–301, http://dx.doi.org/10.1080/14786444108521303.

[7] V. Edwards, J. Newman, The asymmetric Graetz problem in channel flow, Int. J. Heat Mass Transfer 28 (2) (1985) 503–505, http://dx.doi.org/10.1016/0017-9310(85)90085-7.

[8] J. Mitrović, B. Maletić, B. Bačlić, Some peculiarities of the asymmetric Graetz problem, Internat. J. Engrg. Sci. 44 (7) (2006) 436–455, http://dx.doi.org/10.1016/j.ijengsci.2006.02.003.

[9] E. Hicken, Der Wärmeübergang im thermischen Einlauf rechteckiger Kanäle bei nur teilweise beheiztem Umfang, Wärme- und Stoffübertragung 5 (1972) 213–219.

[10] C. Barrera, M. Letelier, D. Siginer, J. Stockle, The Graetz problem in tubes of arbitrary cross section, Acta Mech. 227 (11) (2016) 3239–3246, http://dx.doi.org/10.1007/s00707-015-1540-y.

[11] R.B. Bird, W.E. Stewart, E.N. Lightfoot, Transport Phenomena, Revised second edition, John Wiley & Sons, Inc., New York, 2007.

[12] G.S. Barozzi, G. Pagliarini, A method to solve conjugate heat transfer problems: The case of fully developed laminar flow in a pipe, J. Heat Transf. 107 (1) (1985) 77–83, http://dx.doi.org/10.1115/1.3247406.

[13] C.-T. Liou, F.-S. Wang, Solutions to the extended Graetz problem for a power-model fluid with viscous dissipation and different entrance boundary conditions, Numer. Heat Transf. Part A: Appl. 17 (1) (1990) 91–108, http://dx.doi.org/10.1080/10407789008944734.

[14] M.-P. Errera, R. Moretti, J. Mayeur, M. Gelain, L. Tessé, J.-M. Lamet, E. Laroche, A numerical predictive model for conjugate heat transfer with radiation, Int. J. Heat Mass Transfer 160 (2020) 120155, http://dx.doi.org/10.1016/j.ijheatmasstransfer.2020.120155.

[15] L.J. Slater, D. Lit, Confluent Hypergeometric Functions, Cambridge University Press, 1960.

[16] E. Papoutsakis, D. Ramkrishna, Conjugated Graetz problems—I, Chem. Eng. Sci. 36 (8) (1981) 1381–1391, http://dx.doi.org/10.1016/0009-2509(81)80172-8.

[17] S. Straub, Non-Homogeneous Thermal Boundary Conditions in Low to Medium Prandtl Number Turbulent Pipe Flows (Ph.D. thesis), Karlsruhe, 2020.

[18] J. Neuhauser, `graetz` - a Python package for numerical evaluation of analytical solutions to various versions of the Graetz problem., 2025, URL https://github.com/joneuhauser/graetz, (Accessed 24 March 2025).